NEW VEGETATION INDICES FOR FULL AND COMPACT POLARIMETRIC SAR DATA: IN PREPARATION FOR THE RADARSAT CONSTELLATION MISSION (RCM)

D. Ratha[1], D. Mandal[1], S. Dey[1], A. Bhattacharya[1],*, A. Frery[2,3], Y. S. Rao[1], H. McNairn[4]

[1]Microwave Remote Sensing Lab, Center of Studies in Resources Engineering, IIT Bombay, Mumbai - 400 076, India
[2]Laboratório de Computação Científica e Análise Numérica, Universidade Federal de Alagoas, Maceió, Brazil,
[3]The Key Lab of Intelligent Perception and Image Understanding of the Ministry of Education, Xidian University, Xi'an, China.
[4]Ottawa Research and Development Centre, Agriculture and Agri-Food Canada, 960 Carling Ave, Ottawa, Ontario, Canada.
(*e-mail: {debanshu.ratha, dipankar_mandal, sdey23}@iitb.ac.in, {avikb, ysrao}@csre.iitb.ac.in, acfrery@laccan.ufal.br*)

KEY WORDS: PolSAR, Vegetation, Index, Full-pol, Compact-pol, RADARSAT-2, Geodesic Distance

ABSTRACT:

In this paper, we present two radar vegetation indices for full-pol and compact-pol SAR data, respectively. Both are derived using the notion of a geodesic distance between observation and well-known scattering models available in the literature. While the full-pol version depends on a generalized volume scattering model, the compact-pol version uses the ideal depolariser to model the randomness in the vegetation. We have utilized the RADARSAT Constellation Mission (RCM) time-series data from the SAMPVEX16-MB campaign in the Manitoba region of Canada for comparing and assessing the indices in terms of the change in the biophysical parameters as well. The compact-pol data for comparison is simulated from the full-pol RCM time series. Both the indices show better performance at correlating with biophysical parameters such as Plant Area Index (PAI) and Volumetric Water Content (VWC) for wheat and soybean crops, in comparison to the state-of-art Radar Vegetation Index (RVI) of Kim and van Zyl. These indices are timely for the upcoming release of the data from the RCM, which will provide data in both full and compact-pol modes, aimed at better crop monitoring from space.

1. INTRODUCTION

Vegetation indices are often used as a proxy for plant growth. Recognizing the potential of vegetation indices derived from optical sensors, regional to global products are advocated for operational uses. Similar to the spectral indices that are well established in optical remote sensing, a vegetation index derived from synthetic aperture radar (SAR) data could provide complementary information for crop growth monitoring (van Zyl, 2011; Li, Wang). This information from SAR data is essential when the optical measurements are not practicable considering the cloud cover. The sensitivity of the SAR backscatter signal to vegetation dielectric and geometric properties also gets its due attention from the remote sensing community.

In radar remote sensing application, the Radar Vegetation Index (RVI) (Kim, van Zyl) was introduced as a proxy for plant growth. The RVI was formulated by modeling the vegetation canopy as a collection of randomly oriented dipoles, and it by principal utilizes a measure of scattering randomness from vegetation targets. The RVI is used in several studies (Kim et al., 2012, 2014; Huang et al., 2016) and indicated a good correlation with canopy biophysical parameters. The investigations by Kim et al. (2012) by a comparative analysis of RVI with optical-sensor based indices i.e., Normalized Difference Vegetation Index (NDVI) indeed results in a good correlation between these indices.

Very recently, a new vegetation index (GRVI) has been proposed by Ratha et al. (2019a), which utilizes the notion of a geodesic distance between observation and scattering models in the literature. In particular, the GRVI utilizes the generalized volume scattering model proposed in (Antropov et al., 2011). It has been found to correlate better with biophysical parameters in comparison to the RVI along with altogether avoiding the eigenvalue decomposition approach, which is fundamental to the definition of RVI.

In view of the upcoming constellation of satellites such as the Canadian RADARSAT Constellation Mission (RCM), SAOCOM (TOPSAR with experimental CP-mode), and NISAR (the NASA-ISRO SAR) L- and S-band mission; the study on compact polarimetric (compact-pol) data holds promise for the future. In a recent study, McNairn et al. (2017) showed that the simulated CP parameters are correlated with the Normalized Difference Vegetation Index (NDVI) derived from optical sensors. Homayouni et al. (2019) assessed the volume to odd-bounce scattering power ratio (P_v/P_s) derived from a scattering power decomposition method from simulated CP-SAR data for vegetation condition monitoring. The P_v/P_s ratio shows a good correlation with NDVI and crop biomass for several crop types. However, as the crop canopy attained its peak growth during the end of the vegetative stage and fruit development, the magnitude of P_v/P_s was overestimated relative to that obtained from full-pol data. Nevertheless, these studies confirm that a derived CP-SAR metric similar to NDVI is essential for agricultural applications. Even though the RVI is a good alternative, it is restricted to the use of full-polarimetric SAR data. Thus, there is a need for a radar vegetation index for CP-SAR data.

In this work, inspired by the approach made in formulating the GRVI for full-pol SAR data, a new vegetation index for compact-pol SAR data is proposed. Due to the lack of a volume model, we use the ideal depolariser to model the randomness in the vegetation. The compact-pol (RH-RV) data is simulated from the full-pol RADARSAT-2 data. The comparison in temporal trends of the two indices of common origin and the RVI is made along with important biophysical parameters such as

*Corresponding Author

This contribution has been peer-reviewed. The double-blind peer-review was conducted on the basis of the full paper.
https://doi.org/10.5194/isprs-annals-IV-3-W2-2020-41-2020 | © Authors 2020. CC BY 4.0 License.
Primary publication at IEEE Xplore: https://doi.org/10.1109/LAGIRS48042.2020.9165685

Plant Area Index (PAI) and Vegetation Water Content (VWC). Correlation studies are also conducted in particular for the two major crops of the test site, i.e., wheat and soybean.

2. METHODOLOGY

2.1 Kennaugh matrix

Under monostatic conditions, the 2×2 complex symmetric scattering matrix $\mathbf{S}$ encompasses the full polarimetric information of the backscatter from targets. It is denoted as

$$\mathbf{S} = \begin{bmatrix} S_{\text{HH}} & S_{\text{HV}} \\ S_{\text{VH}} & S_{\text{VV}} \end{bmatrix}, \tag{1}$$

where the subscripts H and V denote horizontal and vertical polarizations, respectively.

In the real domain, the same information expressed in terms of power through the 4×4 real symmetric Kennaugh matrix $\mathbf{K}$ defined as

$$\mathbf{K} = \frac{1}{2}\mathbf{A}^*(\mathbf{S} \otimes \mathbf{S}^*)\mathbf{A}^{-1}, \quad \mathbf{A} = \begin{bmatrix} 1 & 0 & 0 & 1 \\ 1 & 0 & 0 & -1 \\ 0 & 1 & 1 & 0 \\ 0 & j & -j & 0 \end{bmatrix} \tag{2}$$

where $\otimes$ is the Kronecker product, and $j = \sqrt{-1}$.

However, for studying distributed targets, the coherent information in $\mathbf{S}$ is turned into an incoherent measurement by the process of multi-looking. In its new form, the information is captured as a 3×3 complex Hermitian coherency $\mathbf{T}$ (or equivalently covariance $\mathbf{C}$) matrix. The Kennaugh matrix for the incoherent case can also be obtained from the elements of the coherency matrix $\langle[\mathbf{T}]\rangle$ in the following manner:

$$\mathbf{K} = \begin{bmatrix} \frac{T_{11}+T_{22}+T_{33}}{2} & \Re(T_{12}) & \Re(T_{13}) & \Im(T_{23}) \\ \Re(T_{12}) & \frac{T_{11}+T_{22}-T_{33}}{2} & \Re(T_{23}) & \Im(T_{13}) \\ \Re(T_{13}) & \Re(T_{23}) & \frac{T_{11}-T_{22}+T_{33}}{2} & -\Im(T_{12}) \\ \Im(T_{23}) & \Im(T_{13}) & -\Im(T_{12}) & \frac{-T_{11}+T_{22}+T_{33}}{2} \end{bmatrix} \tag{3}$$

where T_{ij} is the (i, j)-th entry of $\mathbf{T}$ and, $\Re$ and $\Im$ denote the real and imaginary parts of a complex number. Thus, polarimetric information in form of coherent $\mathbf{S}$ or incoherent $\mathbf{T}$ can be easily obtained in their corresponding $\mathbf{K}$ matrices using equations (2) and (3) respectively.

Symmetric scatterers such as trihedral (t), cylinder (c), dipole (dp), quarter waves ($\pm 1/4$), narrow dihedral (nd), dihedral (d) and the asymmetric scatterers such as left and right helices (lh and rh) are well studied in PolSAR literature. The Kennaugh matrices of these elementary scatterers, along with the ideal depolarizer (ID) is given in Table 1. These scatterers have been useful for pertinent applications within the PolSAR domain., e.g., in target decompositions, an ocean surface will provide a high trihedral component, while buildings perpendicular to radar line of sight (LoS) will provide a high dihedral component. Thus, using a distance measure to measure the dissimilarity of observations with the models forms the first-hand choice for PolSAR data analysis. In this light, the geodesic distance (GD) on the unit sphere in the space of 4×4 real matrices is found useful in many PolSAR applications Ratha et al. (2019b).

Table 1. Kennaugh Matrices for Elementary Targets and the Ideal Depolarizer

Target	Row 1	Row 2	Row 3	Row 4
$\mathbf{K}_t$	1 0 0 0	0 1 0 0	0 0 1 0	0 0 0 -1
$\mathbf{K}_c$	5/8 3/8 0 0	3/8 5/8 0 0	0 0 1/2 0	0 0 0 -1/2
$\mathbf{K}_{dp}$	1 -1 0 0	-1 1 0 0	0 0 0 0	0 0 0 0
$\mathbf{K}_{-1/4}$	1 0 0 0	0 1 0 0	0 0 0 -1	0 0 -1 0
$\mathbf{K}_{+1/4}$	1 0 0 0	0 1 0 0	0 0 0 1	0 0 1 0
$\mathbf{K}_{nd}$	5/8 3/8 0 0	3/8 5/8 0 0	0 0 -1/2 0	0 0 0 1/2
$\mathbf{K}_d$	1 0 0 0	0 1 0 0	0 0 -1 0	0 0 0 1
$\mathbf{K}_{lh}$	1 0 0 -1	0 0 0 0	0 0 0 0	-1 0 0 1
$\mathbf{K}_{rh}$	1 0 0 1	0 0 0 0	0 0 0 0	1 0 0 1
$\mathbf{K}_{\text{ID}}$	1 0 0 0	0 0 0 0	0 0 0 0	0 0 0 0

2.2 Geodesic Distance

The Kennaugh matrices by definition are 4×4 real matrices. Thus, the GD between two arbitrary Kennaugh matrices ($\mathbf{K}_1$ and $\mathbf{K}_2$) (first proposed in Ratha et al. (2017)) is defined as,

$$GD(\mathbf{K}_1, \mathbf{K}_2) = \frac{2}{\pi} \cos^{-1} \frac{\text{Tr}(\mathbf{K}_1^T \mathbf{K}_2)}{\sqrt{\text{Tr}(\mathbf{K}_1^T \mathbf{K}_1)}\sqrt{\text{Tr}(\mathbf{K}_2^T \mathbf{K}_2)}}, \tag{4}$$

where Tr is the trace operator, and the superscript T denotes transpose. The $2/\pi$ is the normalization factor. The GD is adaptively utilized in several applications in a series of papers by the authors for full-polarimetric SAR data. The GD has several elegant properties such as boundedness, scale invariance, and invariance under the orthogonal transformation of the polarization basis which makes GD quite versatilite for PolSAR applications. A detailed mathematical treatment of the GD along with a survey of its past and future applications is presented in Ratha et al. (2019b).

2.3 Generalized Volume RVI (GRVI)

Vegetation is a distributed target, and finding a model with a good-fit has been a challenge in PolSAR literature. Hence, we can find several volume scattering models to represent the scattering from vegetation. This makes the choice of volume scattering model for vegetation studies a dilemma for researchers within the field. Recently, a parameterized generalized volume model was proposed by Antropov et al. (2011). It depends on two parameters, namely the co-polarized channel ratio (γ) and the co-polarized channel correlation coefficient (ρ). For practical purposes, ρ is fixed at $1/3$. The Kennaugh matrix $\mathbf{K}_{\text{GV}}$ expressed in form of γ in equation (5). This generalized volume model provides many of the prevalent volume scattering models in PolSAR literature as its special cases. In Ratha et al. (2019a), the geodesic distance of the observation with the generalized volume model, as well as the geodesic distances from even and odd bounce scatterers was synergistically combined to propose a radar vegetation index (GRVI) for full-pol SAR data.

$$\text{GRVI} = \beta\, f_{\text{GV}}, \quad 0 \leq \text{GRVI} \leq 1, \tag{6}$$

$$f_{\text{GV}} = (1 - GD_{\text{GV}}), \quad \beta = \left(\frac{p}{q}\right)^{2\,GD_{\text{GV}}}, \tag{7}$$

$$p = \min \begin{bmatrix} GD(\mathbf{K}, \mathbf{K}_t) \\ GD(\mathbf{K}, \mathbf{K}_c) \\ GD(\mathbf{K}, \mathbf{K}_d) \\ GD(\mathbf{K}, \mathbf{K}_{nd}) \end{bmatrix}, q = \max \begin{bmatrix} GD(\mathbf{K}, \mathbf{K}_t) \\ GD(\mathbf{K}, \mathbf{K}_c) \\ GD(\mathbf{K}, \mathbf{K}_d) \\ GD(\mathbf{K}, \mathbf{K}_{nd}) \end{bmatrix} \tag{8}$$

This contribution has been peer-reviewed. The double-blind peer-review was conducted on the basis of the full paper.
https://doi.org/10.5194/isprs-annals-IV-3-W2-2020-41-2020 | © Authors 2020. CC BY 4.0 License.
Primary publication at IEEE Xplore: https://doi.org/10.1109/LAGIRS48042.2020.9165685

$$\mathbf{K}_{\text{GV}} = \frac{1}{\frac{3(1+\gamma)}{4} - \frac{\sqrt{\gamma}}{6}} \begin{bmatrix} \frac{3}{2}(1+\gamma) - \frac{\sqrt{\gamma}}{3} & \gamma - 1 & 0 & 0 \\ \gamma - 1 & \frac{1}{2}(1+\gamma) + \frac{\sqrt{\gamma}}{3} & 0 & 0 \\ 0 & 0 & \frac{1}{2}(1+\gamma) + \frac{\sqrt{\gamma}}{3} & 0 \\ 0 & 0 & 0 & \frac{1}{2}(1+\gamma) - \sqrt{\gamma} \end{bmatrix} \tag{5}$$

The two extreme cases, viz., GRVI $= 0$ and GRVI $= 1$ correspond to $\mathbf{K} \in \{\mathbf{K}_t, \mathbf{K}_c, \mathbf{K}_d, \mathbf{K}_{nd}\}$ and $\mathbf{K} = \mathbf{K}_{\text{GV}}$, respectively. The role of the β is as a damping factor which will bring down the GRVI value for non-vegetation zones in which one of the odd or even bounce scattering is dominant.

The GRVI was compared with eigenvalue based RVI in respect of its correlation with biophysical parameters such as VWC (Volumetric Water Content), and the PAI (Plant Area Index). There was no assumption made on the mode of polarization while computing the GD between Kennaugh matrices. Hence, the definition holds for Kennaugh matrices obtained in the hybrid compact polarimetric mode, as well.

2.4 Compact-pol RVI (CpRVI)

In the hybrid compact polarimetric mode the earlier $\mathbf{S}$ matrix representation is replaced with the scattering vector given as

$$\begin{bmatrix} E_{CH} \\ E_{CV} \end{bmatrix} = \frac{1}{\sqrt{2}} \begin{bmatrix} S_{HH} & S_{HV} \\ S_{VH} & S_{VV} \end{bmatrix} \begin{bmatrix} 1 \\ \pm i \end{bmatrix} \tag{9}$$

$$= \frac{1}{\sqrt{2}} \begin{bmatrix} S_{HH} \pm iS_{HV} \\ S_{VH} \pm iS_{VV} \end{bmatrix} \tag{10}$$

where the subscript C can be either the left-hand circular (LHC) transmit with a + sign or the right-hand circular (RHC) transmit with a - sign. For the incoherent case, the covariance matrix is then obtained from the elements of the scattering vector as a 2×2 complex Hermitian matrix,

$$\langle[\mathbf{C}]\rangle = \begin{bmatrix} \langle|E_{CH}|^2\rangle & \langle E_{CH}E_{CV}^*\rangle \\ \langle E_{CV}E_{CH}^*\rangle & \langle|E_{CV}|^2\rangle \end{bmatrix} \tag{11}$$

For CP-SAR data, the 4×1 Stokes vector $\vec{\mathbf{g}}$ can be written in terms of the elements $\mathbf{C}$ as,

$$\vec{\mathbf{g}} = \begin{bmatrix} g_0 \\ g_1 \\ g_2 \\ g_3 \end{bmatrix} = \begin{bmatrix} C_{11} + C_{22} \\ C_{11} - C_{22} \\ C_{12} + C_{21} \\ \pm j\,(C_{12} - C_{21}) \end{bmatrix}, \tag{12}$$

where $\pm$ corresponds to left and right circular polarization respectively. The Kennaugh matrix ($\mathbf{K}_{\text{CP}}$) for CP-data can be written in terms of the elements of the Stokes vector as,

$$\mathbf{K}_{\text{CP}} = \begin{bmatrix} g_0 & 0 & g_2/2 & 0 \\ 0 & 0 & 0 & g_1 \\ g_2/2 & 0 & 0 & 0 \\ 0 & g_1 & 0 & g_3/2 \end{bmatrix}. \tag{13}$$

As such there does not exist volume scattering model for CP-SAR data. Thus, we utilize the ideal depolarizer (ID) to model the randomness from distributed targets.

In defining the GRVI in (6), the imbalance in the similarity of observation with odd (t, c) and even bounce scatterers (nd, d) is utilized. This will be facilitated in the CP-SAR case by considering the imbalance between received backscattering power in the opposite sense (OC) and the same sense (SC), respectively.

To define a similarity of observation with the ideal depolarizer, it may be noted that $GD_{\text{ID}} = GD(\mathbf{K}, \mathbf{K}_{\text{ID}})$ has a upper theoretical limit of 2/3. Thus, the similarity $f_{\text{ID}} = 1 - (3/2)GD_{\text{ID}}$ is defined accordingly to obtain a range of [0 1].

In this light, we propose a novel Compact-pol Radar Vegetation Index is defined as

$$\text{CpRVI} = \beta\, f_{\text{ID}}, \quad 0 \le \text{CpRVI} \le 1, \tag{14}$$

$$f_{\text{ID}} = 1 - (3/2)GD_{\text{ID}}, \quad \beta = \left(\frac{p}{q}\right)^{2\,(3/2\,GD_{\text{ID}})}, \tag{15}$$

$$p = \min\{\text{SC}, \text{OC}\}, \quad q = \max\{\text{SC}, \text{OC}\}, \tag{16}$$

$$\text{SC} = \frac{(g_0 - g_3)}{2}, \quad \text{OC} = \frac{(g_0 + g_3)}{2}, \tag{17}$$

where g_0 (the 1st element of $\vec{\mathbf{g}}$) is the total average received power and g_3 (the 4th element) is a measure of the average received power in circular polarization. Hence, the role of β is exactly the same as in case of GRVI.

The proportion of the power that is received by the radar in opposite-sense circular polarization to that transmitted is OC $= (g_0 + g_3)/2$. When the EM wave undergoes odd number reflections, such a change in polarity occurs. Similarly, SC $= (g_0 - g_3)/2$ is the power received by the radar in the same-sense circular polarization as it was transmitted, which is a case for an even number of reflections. Thus the role of β is similar to that of the damping factor used in GRVI.

The two extreme cases, viz., CpRVI $= 0$ and CpRVI $= 1$ correspond to a coherent target (observation correspondg to a $\mathbf{S}$) and $\mathbf{K} = \mathbf{K}_{\text{ID}}$, respectively.

3. DATASET AND STUDY AREA

This work is conducted over the Joint Experiment for Crop Assessment and Monitoring (JECAM) test site in Carman, Manitoba (Canada). This area is considered as one of the supersite of the Joint Experiment for Crop Assessment and Monitoring (JECAM) network. The average extent of the test area is $26{\times}48\,\text{km}^2$ as shown in Fig. 1. The annual crop inventory map indicates four major crop wheat, soybean, canola, and oats, which are grown in the area (Fig. 2). The seeding of annual crops in Manitoba started at the end of April to mid-May and harvesting in August. The in-situ measurements were collected over the area with near coincident satellite passes as a part of the Soil Moisture Active Passive Validation Experiment 2016 (SMAPVEX16-MB) campaign (Bhuiyan et al., 2018). In-situ sampling was conducted, which included measurement of plant area index (PAI), wet and dry biomass, plant height, plant density, and phenology through destructive and non-destructive methods (Mcnairn et al., 2016; Bhuiyan et al., 2018). Table 2 provides information about the satellite passes, which has been utilized in this study.

This contribution has been peer-reviewed. The double-blind peer-review was conducted on the basis of the full paper.
https://doi.org/10.5194/isprs-annals-IV-3-W2-2020-41-2020 | © Authors 2020. CC BY 4.0 License.
Primary publication at IEEE Xplore: https://doi.org/10.1109/LAGIRS48042.2020.9165685

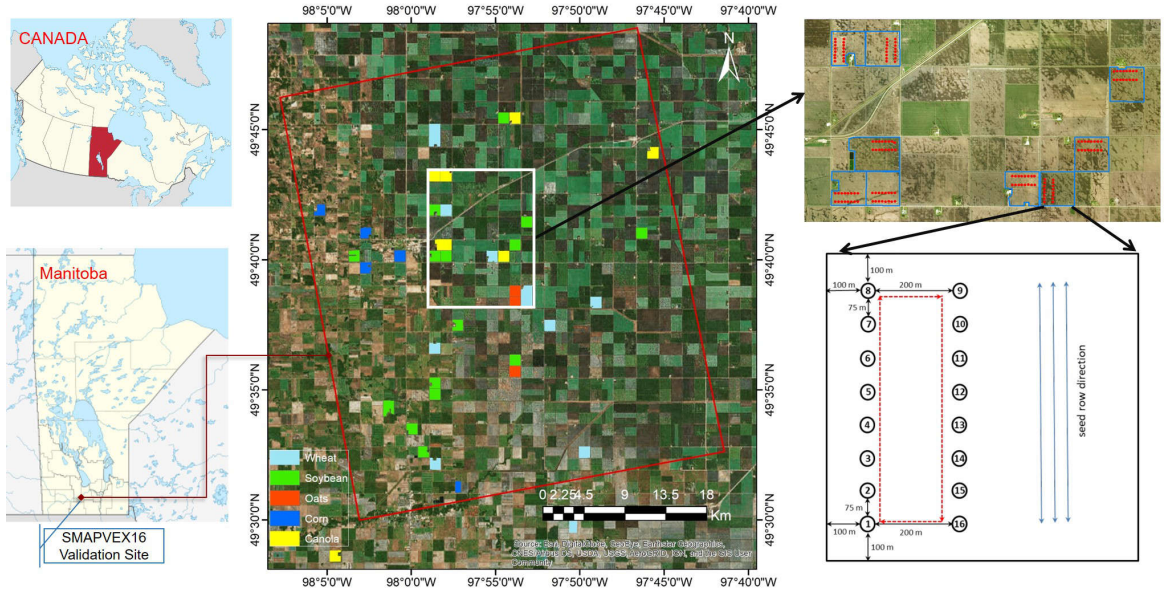

Figure 1. Study area and sampling locations over the JECAM-Manitoba (Canada) test site. The layout of the sampling locations within each field is highlighted for vegetation sampling.

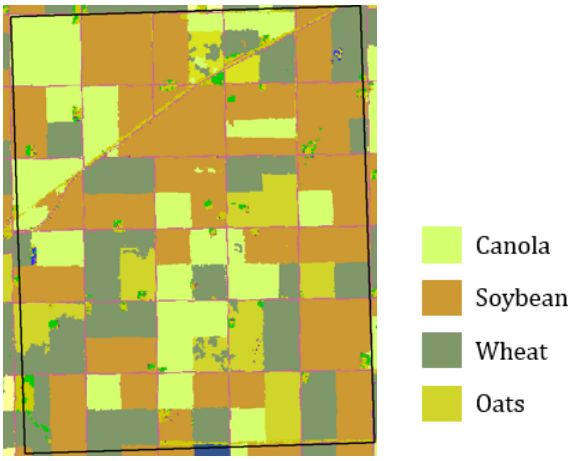

(a) Crop Inventory Map (b) Crop Legend

Figure 2. Crop inventory map over the test site at Carman, Canada for 2016 crop season.

4. RESULTS AND DISCUSSION

The vegetation indices (both the GRVI and RVI) for different sampling sites are generated from the RADARSAT-2 quad-pol data set. VI values for each sampling location (point measurements) are extracted over a 3×3 window, and the temporal analysis is performed at different growth stages. The temporal variation of the three vegetation indices (i.e., RVI, GRVI, and CpRVI) for the scene are shown in Fig. 2. The three vegetation indices are compared for different phenological stages of wheat and soybean, as shown in Fig. 4. From several sampling sites, 3 representative fields (field numbers: 220, 105, 233 for wheat; and 113, 82, 232 for soybean) for each crop are used for the temporal analysis of vegetation indices. It can be observed that the temporal trend follows PAI and VWC for both wheat and soybean. The growth trends of the vegetation indices are similar irrespective of plant density among several fields, i.e., an increase of PAI and VWC with crop development. However, the RVI, GRVI, and CpRVI values for field no.105 are comparatively higher for all phenological observations, which have the highest plant density-PD (approximately 230 plants/m^2). In the other two fields, separation of CpRVI, GRVI, and RVI values within a field becomes apparent (Fig. 4) when wheat has advanced from the leaf development to booting and start of the flowering stage.

Table 2. Specifications of RADARSAT-2 data acquisitions

Acquisition date	Beam Mode	Incidence Angle Range (deg.)	Orbit
30/05/2016	FQ7W	24.98–28.32	Ascending
15/06/2016	FQ7W	24.98–28.32	Descending
23/06/2016	FQ7W	24.98–28.32	Ascending
09/07/2016	FQ7W	24.98–28.32	Descending
17/07/2016	FQ7W	24.98–28.32	Ascending
02/08/2016	FQ7W	24.98–28.32	Descending

CpRVI values reached their maximum when crop advanced from stem elongation to early dough or fruit development stages on 17 July. CpRVI values reach up to 0.65 for low PD fields, while these values peak at ≈0.8 for high PD wheat fields. This variation may be due to the high degree of randomness in scattering from the canopy elements during the flowering to fruit development stages. Unlike CpRVI, which follows almost a monotonic increase along phenological stages, the fluctuation of RVI values is more apparent. It is possibly due to the inherent noise that arises in the numerator term of RVI formulation, i.e., the third eigenvalue, which is more affected by noise rather than changes in vegetation randomness (Mandal et al., 2020). However, the GRVI values are more stable than the RVI and CpRVI.

Unlike the RVI, which models the vegetation layer as an aggregation of randomly oriented dipoles, the GRVI offers the flexibility to choose the parameters of the generalized volume scattering model (GVSM) from the measured data to describe the volume scattering model Ratha et al. (2019a). In this way, the GVSM might capture the phenological changes within a volume model, whereas both the CpRVI and RVI lacks this aspect. On the contrary, in the absence of any volume scattering models to suitably describe scattering from vegetation in CP-SAR data, the ideal depolarizer (ID) is utilized to measure randomness from distributed targets in CpRVI. Moreover, the

This contribution has been peer-reviewed. The double-blind peer-review was conducted on the basis of the full paper.
https://doi.org/10.5194/isprs-annals-IV-3-W2-2020-41-2020 | © Authors 2020. CC BY 4.0 License.
Primary publication at IEEE Xplore: https://doi.org/10.1109/LAGIRS48042.2020.9165685

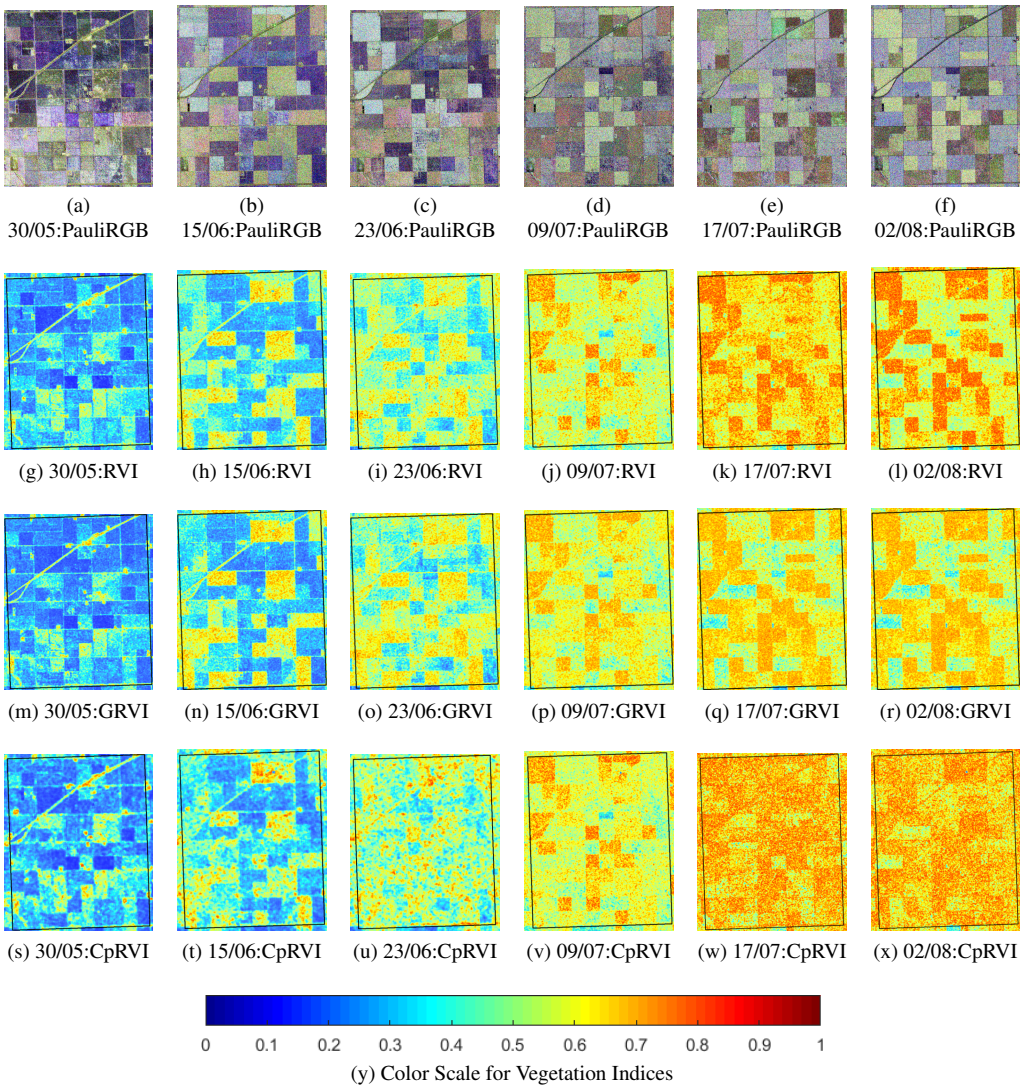

Figure 3. Evolution of Pauli RGB and the vegetation indices over time.

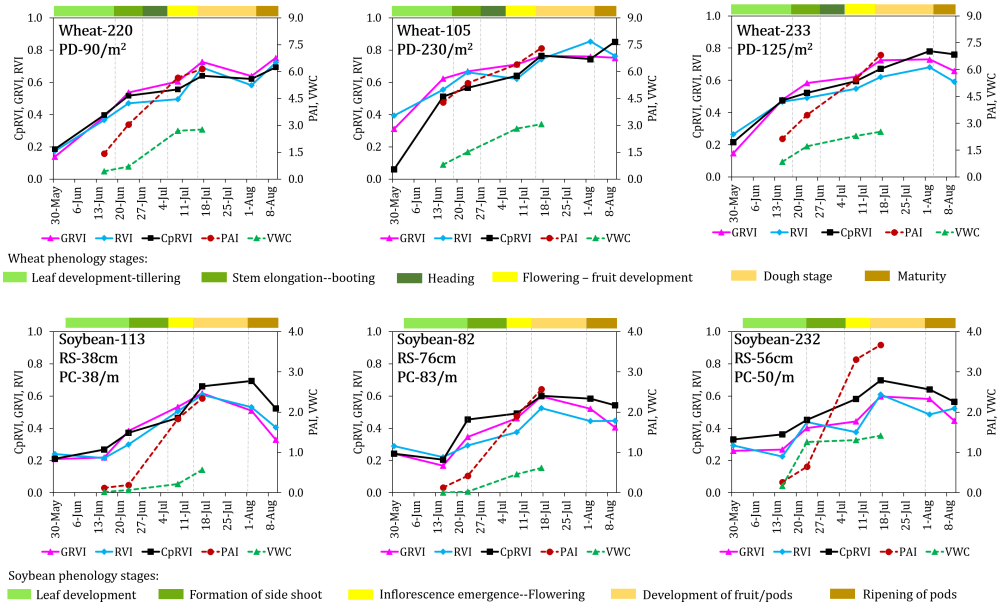

Figure 4. Temporal pattern of vegetation indices (CpRVI, RVI, and GRVI) for wheat and soybean fields.

This contribution has been peer-reviewed. The double-blind peer-review was conducted on the basis of the full paper.
https://doi.org/10.5194/isprs-annals-IV-3-W2-2020-41-2020 | © Authors 2020. CC BY 4.0 License.
Primary publication at IEEE Xplore: https://doi.org/10.1109/LAGIRS48042.2020.9165685

geodesic distances from the odd (i.e., trihedral) and the even bounce (i.e., dihedral) scatterers that appear in GRVI Ratha et al. (2019a) is suitably replaced by the received echo powers from the same circular (SC) and the opposite circular (OC) sense to the transmitted polarization.

The variations with CpRVI and RVI values are more apparent in the low biomass soybean crop. Fig. 4 presents the temporal trends of CpRVI and RVI for three representative soybean fields with different row spacing (RS) and plant count per meter length (PC). Both the CpRVI and RVI values for each field increase as the vegetation growth increases from the early vegetative growth stages to the beginning of pod development. With the increase in vegetation components, the differential increase in CpRVI and RVI values among several fields are apparent.

With the increase in vegetation components, the differential increase in vegetation indices values among several fields is apparent. The correlation analysis of vegetation indices with crop biophysical parameters given in Table 3. The correlation coefficient (r) of CpRVI with PAI is 0.72 and 0.85, which is higher than that of RVI ($r = 0.68$ and 0.76) for wheat and soybean. A similar improvement of r is observed for VWC for both the crops. The correlation analysis shows marginally better performance of CpRVI compared to RVI, while it is inferior to GRVI for characterizing vegetation growth.

Table 3. Correlation of Vegetation Indices with PAI and VWC for wheat and soybean.

Crop	Vegetation parameter	Correlation coefficient (r)		
		CpRVI	GRVI	RVI
Wheat	PAI	0.72	0.77	0.68
	VWC	0.62	0.71	0.60
Soybean	PAI	0.85	0.92	0.76
	VWC	0.75	0.82	0.74

5. CONCLUSION

Two vegetation indices for full polarimetric and compact polarimetric SAR have been respectively presented in this study. The temporal analysis of the proposed indices derived from the simulated RCM data suggests that it has a positive correlation with the crop growth development parameters, i.e., Plant Area Index (PAI) and vegetation water content (VWC). Notably, the proposed vegetation indices hold significant interest from an operational perspective for upcoming SAR missions, e.g., the RADARSAT Constellation Mission (RCM).

ACKNOWLEDGEMENTS

The authors would like to thank the Canadian Space Agency and MAXAR Technologies Ltd. (formerly MDA) for providing RADARSAT-2 data to the SMAPVEX16-MB research team. Authors acknowledge the GEO-AWS Earth Observation Cloud Credits Program, which supported the computation on AWS cloud platform through the project "AWS4AgriSAR-Crop inventory mapping from SAR data on cloud computing platform". D. Ratha would like to acknowledge the support of CSIR, Govt. of India, towards doctoral studies.

References

Antropov, O., Rauste, Y., Hame, T., 2011. Volume Scattering Modeling in PolSAR Decompositions: Study of ALOS PALSAR Data Over Boreal Forest. *IEEE Trans. Geosci. Remote Sens.*, 49(10), 3838-3848.

Bhuiyan, H. A., McNairn, H., Powers, J., Friesen, M., Pacheco, A., Jackson, T. J., Cosh, M. H., Colliander, A., Berg, A., Rowlandson, T. et al., 2018. Assessing SMAP Soil Moisture Scaling and Retrieval in the Carman (Canada) Study Site. *Vadose Zone Journal*, 17(1).

Homayouni, S., McNairn, H., Hosseini, M., Jiao, X., Powers, J., 2019. Quad and compact multitemporal C-band PolSAR observations for crop characterization and monitoring. *Int. J. Appl. Earth Observ. Geoinf.*, 74, 78–87.

Huang, Y., Walker, J. P., Gao, Y., Wu, X., Monerris, A., 2016. Estimation of Vegetation Water Content From the Radar Vegetation Index at L-Band. *IEEE Trans. Geosci. Remote Sens.*, 54(2), 981-989.

Kim, Y., Jackson, T., Bindlish, R., Hong, S., Jung, G., Lee, K., 2014. Retrieval of wheat growth parameters with radar vegetation indices. *IEEE Geosci. Remote Sens. Lett.*, 11(4), 808–812.

Kim, Y., Jackson, T., Bindlish, R., Lee, H., Hong, S., 2012. Radar vegetation index for estimating the vegetation water content of rice and soybean. *IEEE Geosci. Remote Sens. Lett.*, 9(4), 564–568.

Kim, Y., van Zyl, J. J., 2009. A time-series approach to estimate soil moisture using polarimetric radar data. *IEEE Trans. Geosci. Remote Sens.*, 47(8), 2519-2527.

Li, J., Wang, S., 2018. Using SAR-Derived Vegetation Descriptors in a Water Cloud Model to Improve Soil Moisture Retrieval. *Remote Sensing*, 10(9), 1370.

Mandal, D., Kumar, V., Ratha, D., Lopez-Sanchez, J. M., Bhattacharya, A., McNairn, H., Rao, Y., Ramana, K., 2020. Assessment of rice growth conditions in a semi-arid region of India using the Generalized Radar Vegetation Index derived from RADARSAT-2 polarimetric SAR data. *Remote Sensing of Environment*, 237, 111561.

Mcnairn, H. et al., 2016. Experimental plan SMAP validation experiment 2016 in Manitoba, Canada (SMAPVEX16-MB).

McNairn, H., Homayouni, S., Hosseini, M., Powers, J., Beckett, K., Parkinson, W., 2017. Compact polarimetric synthetic aperture radar for monitoring crop condition. *Proc. IEEE Int. Geosci. Remote Sens. Symp.*, IEEE, 4358–4361.

Ratha, D., De, S., Celik, T., Bhattacharya, A., 2017. Change Detection in Polarimetric SAR Images Using a Geodesic Distance Between Scattering Mechanisms. *IEEE Geosci. Remote Sens. Lett.*, 14(7), 1066-1070.

Ratha, D., Mandal, D., Kumar, V., McNairn, H., Bhattacharya, A., Frery, A. C., 2019a. A Generalized Volume Scattering Model-Based Vegetation Index From Polarimetric SAR Data. *IEEE Geosci. Remote Sens. Lett.*, 1-5.

Ratha, D., Pottier, E., Bhattacharya, A., Frery, A. C., 2019b. A PolSAR Scattering Power Factorization Framework and Novel Roll-Invariant Parameter-Based Unsupervised Classification Scheme Using a Geodesic Distance. *IEEE Transactions on Geoscience and Remote Sensing*.

van Zyl, J. J., 2011. *Synthetic aperture radar polarimetry*. 2, John Wiley & Sons.